Chinese Chemical Letters 32 (2021) 2833–2836

Contents lists available at ScienceDirect

Chinese Chemical Letters

journal homepage: www.elsevier.com/locate/cclet

Communication

Highly ordered Nb_2O_5 nanochannel film with rich oxygen vacancies for electrocatalytic N_2 reduction: Inactivation and regeneration of electrode

Jialu Wang[a,b], Shenghong Kang[a,*], Xiaoguang Zhu[a], Guozhong Wang[a], Haimin Zhang[a,*]

[a] Key Laboratory of Materials Physics, Centre for Environmental and Energy Nanomaterials, Anhui Key Laboratory of Nanomaterials and Nanotechnology, Institute of Solid State Physics, Chinese Academy of Sciences, Hefei 230031, China
[b] University of Science and Technology of China, Hefei 230026, China

ARTICLE INFO

Article history:
Received 26 September 2020
Received in revised form 19 November 2020
Accepted 11 January 2021
Available online 15 January 2021

Keywords:
Niobium oxide (Nb_2O_5)
Nitrogen (N_2) reduction reaction (NRR)
Electrochromism
Oxygen vacancies
Phase transformation

ABSTRACT

We report the fabrication of highly ordered Nb_2O_5 nanochannel film (Nb_2O_5-NCF) onto niobium foil by an anodization method. After thermal treatment, the obtained Nb_2O_5-NCF with rich oxygen vacancies exhibits electrochemical N_2 reduction reaction (NRR) activity with an NH_3 yield rate of 2.52×10^{-10} mol cm^{-2} s^{-1} and a faradaic efficiency of 9.81% at −0.4 V (*vs.* RHE) in 0.1 mol/L Na_2SO_4 electrolyte (pH 3.2). During electrocatalytic NRR, the Nb_2O_5-NCF takes place electrochromism (EC), along with a crystalline phase transformation from *pseudo* hexagonal phase to hexagonal phase owing to H^+ insertion. This results in the reduced NRR activity due to the decrease of oxygen vacancies of hexagonal phase Nb_2O_5, which can be readily regenerated by low-temperature thermal treatment or applying an anodic potential, showing superior recycling reproducibility.

Ammonia (NH_3) as very important chemical has been widely applied in fuel of vehicles, agricultural, plastic and textile industries [1–4]. Although abundant nitrogen (N_2) exists in the atmosphere (~78%), efficient utilization of N_2 is still very difficult due to high energy barrier for N≡N bond cleavage (~941 kJ/mol), large energy gap (~10.82 eV), and the lowest unoccupied molecular orbital [5]. The synthesis of NH_3 by N_2 hydrogenation is a complex reduction process with multiple reactions [6–8]. Industrially, the NH_3 production from N_2 and H_2 was performed at high temperature (400–600 °C) and pressure (20–40 MPa) by the well-known Haber-Bosch process [9–12], consuming enormous energy and concurrently releasing a large amount of CO_2. Therefore, development of environmentally friendly NH_3 synthesis techniques at ambient conditions is highly desirable.

Electrocatalytic N_2 reduction reaction (NRR) at ambient conditions has been regarded as a promising NH_3 synthesis method for replacing the traditional energy- and capital-intensive Haber-Bosch process [9–12]. To date, varieties of electrocatalysts have been synthesized and applied in electrocatalytic NRR to synthesize NH_3, such as noble metal catalysts [13,14], non-precious metal catalysts [15,16] and metal-free carbon catalysts [17–19], demonstrating high NRR activities. Among non-precious metal catalysts, transition metal oxides have been proven to be efficient catalysts toward electrocatalytic NRR to NH_3, confirming the oxygen vacancies (V_o) as the active centers [20–24]. As we know, niobium oxides have become important materials for catalysis applications [25] because of their superior catalytic activity and high physical/chemical stability. Recently, Kong *et al.* [26] reported Nb_2O_5 nanowires array as high-performance NRR electrocatalyst, demonstrating an NH_3 yield rate of 1.58×10^{-10} mol s^{-1} cm^{-2} with a Faradaic efficiency (FE) of 2.26%. In their work, this good NRR activity can be ascribed to the important role of (001) facet of Nb_2O_5. The Nb_2O_5 nanofiber with high conductivity was also synthesized by Han and co-workers for electrocatalytic NRR to NH_3 [27], showing an NH_3 yield rate of 43.6 μg h^{-1} $mg_{cat.}^{-1}$ with an FE of 9.26%. In their study, this high NRR activity is mainly resulted from Nb-edge atoms of Nb_2O_5 (181) surface to polarize and activate N_2 molecules. It is well known that *pseudo* hexagonal phase Nb_2O_5 has been confirmed to contain rich V_o [28], which could be a promising candidate as the electrocatalyst for NRR to NH_3. In particular, pseudo hexagonal phase Nb_2O_5 nanostructured arrays (*e.g.*, nanochannel array) could provide more excellent electron transfer pathways with exposed V_o active sites for high-efficiency NRR [29,30].

Herein, highly ordered Nb_2O_5 nanochannel film (Nb_2O_5-NCF) was fabricated on niobium foil substrate by a facile anodization

* Corresponding authors.
E-mail addresses: shkang@issp.ac.cn (S. Kang), zhanghm@issp.ac.cn (H. Zhang).

https://doi.org/10.1016/j.cclet.2021.01.020
1001-8417/

method. After thermal treatment in air, the as-fabricated Nb_2O_5-NCF with *pseudo* hexagonal phase contains rich oxygen vacancy defects, as the free-standing electrode, displaying high electrocatalytic NRR activity with an NH_3 yield rate of 2.52×10^{-10} mol cm^{-2} s^{-1} and an FE of 9.81% at −0.4 V (*vs.* RHE) in 0.1 mol/L Na_2SO_4 solution (pH 3.2). During electrocatalytic NRR, it was found that the crystalline phase transformation of Nb_2O_5-NCF from *pseudo* hexagonal phase to hexagonal phase resulted in the electrochromism (EC) phenomenon and the decrease of NRR activity. This is mainly due to the decrease of V_o in hexagonal phase Nb_2O_5. The used Nb_2O_5-NCF electrode can be readily regenerated by low-temperature thermal treatment or applying an anodic potential, regaining high NH_3 yield rate and FE with superior recycling reproducibility.

After anodization, the surface of niobium (Nb) foil showed dark brown and the surface colour of Nb foil became white after further treating in air at 450 °C (Fig. S1 in Supporting information). The XRD patterns (Fig. 1a) of the thermally treated sample exhibit a *pseudo* hexagonal phase (TT-phase) Nb_2O_5 (JCPDS No. 28-0317) [28]. The SEM images (Figs. 1b and c) show that the surface of the sample possesses porous structure, and a highly ordered nanochannel film with a thickness of ~2.0 μm forms on the Nb foil substrate (denoted as Nb_2O_5-NCF). The TEM image and selected area electron diffraction (SAED) patterns of the sample (Fig. 1d) confirm that the nanochannel walls are polycrystalline structure and the lattice fringes with interplanar distance of 3.12 Å can be ascribed to the (100) plane of TT-phase Nb_2O_5. The surface survey XPS spectrum of Nb_2O_5-NCF sample was provided in Fig. S2a (Supporting information), exhibiting Nb and O elements. The high-resolution Nb 3d XPS spectrum (Fig. S2b in Supporting information) indicates that the Nb 3d peaks at 209.6 and 206.9 eV can be assigned to Nb_2O_5 [31,32].

In this work, the fabricated Nb_2O_5-NCF was directly used as the cathodic electrode for NRR evaluation in 0.1 mol/L Na_2SO_4 solution (pH 3.2) using an H-type electrochemical cell. The linear sweep voltammograms (LSV) results (Fig. 2a) show that the cathodic current density of Nb_2O_5-NCF electrode in N_2-saturated electrolyte is obviously larger than that obtained in Ar-saturated electrolyte when increasing applied potential from −0.3 V to −0.9 V, confirming good NRR activity of Nb_2O_5-NCF. Next, we investigated the influence of applied potential on the NRR performance of Nb_2O_5-NCF. During electrocatalytic NRR, the produced NH_3 and/or N_2H_4 were determined by the indophenol blue [33] and Watt/

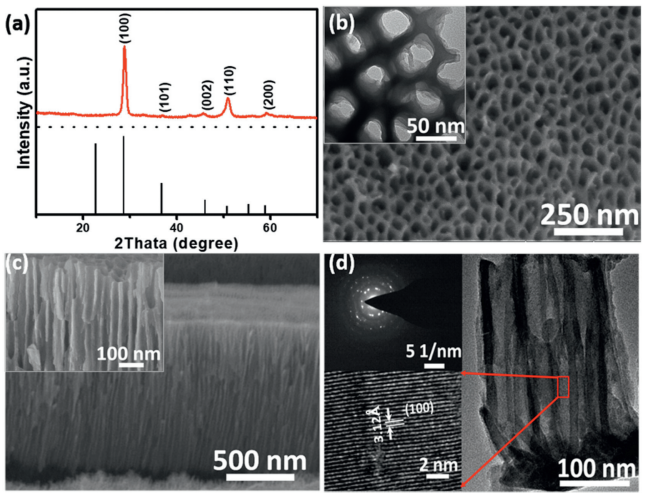

Fig. 1. (a) XRD pattern of Nb_2O_5-NCF. (b) Surface and (c) cross-sectional SEM images of Nb_2O_5-NCF. (d) TEM image and selected area electron diffraction (SAED) patterns for Nb_2O_5-NCF.

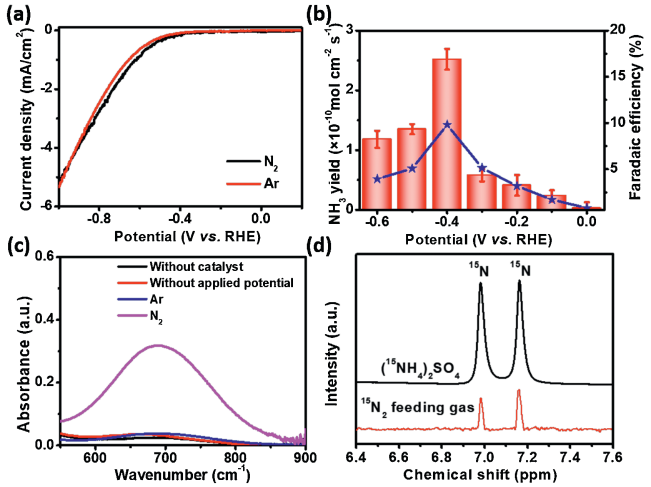

Fig. 2. (a) LSV curves under Ar- or N_2-saturated 0.1 mol/L Na_2SO_4 solution. (b) NH_3 yield rate and FE of Nb_2O_5-NCF at different potentials. (c) UV–vis absorption spectra using the indophenol blue determination method under different conditions. (d) ^1H NMR spectra for $^{15}NH_4^+$ in electrolyte using $^{15}N_2$ as the feeding gas.

Chrisp method [34], respectively. In this work, only NH_3 product can be detected (Fig. S3 in Supporting information) while N_2H_4 is undetectable (Fig. S4 in Supporting information). Fig. 2b shows the NH_3 yield rate and Faradaic efficiency (FE) of Nb_2O_5-NCF at different potentials, and corresponding chronoamperometric curves at each potential are shown in Fig. S5 (Supporting information). According to the UV–vis absorption spectra analysis (Fig. S3a) of NRR samples, the largest NH_3 yield rate can reach 2.52×10^{-10} mol cm^{-2} s^{-1} with an FE of 9.81% at −0.4 V (*vs.* RHE) with the NRR time of 60 min (Fig. 2b). When the applied potential is more negative than −0.4 V (*vs.* RHE), the NRR performance of Nb_2O_5-NCF obviously decreases. This is mainly due to the competitive hydrogen evolution reaction (HER) concurrently happened on Nb_2O_5-NCF at more negative potentials [27]. To eliminate the environmental interference on the NH_3 yielded during NRR, several control experiments were performed. The results (Fig. 2c) show that no NH_3 product can be detected in 0.1 mol/L Na_2SO_4 solution without catalyst, with Nb_2O_5-NCF but without applied potential, or Ar-saturated electrolyte with Nb_2O_5-NCF at −0.4 V (*vs.* RHE), indicating no environmental interference on the produced NH_3 by NRR process. In contrast, the UV–vis absorption spectra show stronger absorption peak at ~695 nm ascribed to the yielded NH_3 determined by the indophenol blue method. To further confirm this, the isotopic labelling experiments using $^{15}N_2$ as the feeding gas was also conducted. The ^1H nuclear magnetic resonance (NMR) spectra (Fig. 2d) reveal that the chemical shift of doublet coupling can be observed for the NRR sample, due to ^{15}N in $^{15}NH_4^+$, suggesting the formed NH_3 indeed originated from the Nb_2O_5-NCF catalyzed NRR process.

Subsequently, we evaluated the durability of Nb_2O_5-NCF electrode for NRR. It was found that the yielded NH_3 amount during NRR initially rapidly increased. After 20 min, the increase trend of NH_3 yield became slow (Fig. S6 in Supporting information). This results in an initial increase then decrease of NH_3 yield rate, and the largest NH_3 yield rate was obtained to be 3.38×10^{-10} mol cm^{-2} s^{-1} with an FE of 11.2% at -0.4 V (*vs.* RHE) (Fig. 3a) when NRR time of 20 min. The above experimental results suggested that the NRR activity of Nb_2O_5-NCF decreased after 20 min of reaction, which deserves a further investigation. During electrocatalytic NRR, the Nb_2O_5 electrode was found to transform to NbO_2 species from XRD results (Fig. 3b), and electrochromism (EC) phenomenon was also observed, namely, the electrode surface color changed from white to dark with NRR time (Fig. 3c). This is mainly

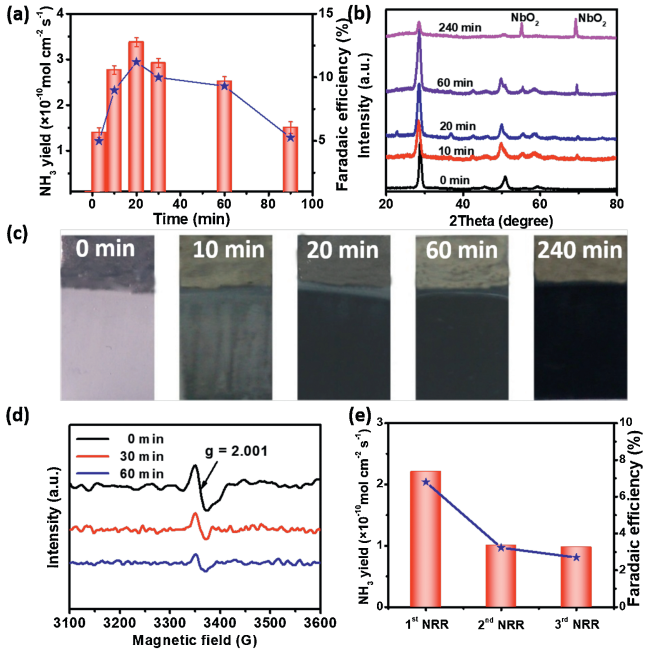

Fig. 3. (a) Time-dependence NH_3 yield rate and FE during continuous NRR. (b) XRD patterns at different times during NRR. (c) The color change of Nb_2O_5-NCF with different reaction times during NRR. (d) EPR spectroscopy of V_o under different NRR times. (e) Recycling experiments using the used Nb_2O_5-NCF electrode with fresh 0.1 mol/L Na_2SO_4 electrolyte after 20 min of NRR for each cycle.

attributed to H^+ ions insertion into the interlayer spacing of TT-phase Nb_2O_5, resulting in the crystalline phase transformation of Nb_2O_5 from TT-phase to T-phase, concurrently accompanied by part of Nb^{5+} reduction to Nb^{4+}, thus the generation of EC phenomenon [35]. Seen from the XRD results of Nb_2O_5-NCF electrode with NRR time (Fig. 3b), compared to the pristine Nb_2O_5-NCF, the (100) diffraction peaks of Nb_2O_5-NCF with different NRR times apparently shift toward low angel direction in the XRD patterns, suggesting H^+ ions insertion into interlayer spacing of Nb_2O_5 [36]. As we know, TT-phase Nb_2O_5 possesses more oxygen vacancies (V_o) than T-phase Nb_2O_5 [28]. These oxygen vacancies have been proven to be the catalytic active sites for N_2 adsorption, activation and hydrogenation [26,27]. The N_2 firstly adsorbed on V_o sites of N_2O_5, and V_o-induced bands in Nb_2O_5 concurrently provided defect states for trapping excited electrons. Then these electrons were transferred and exchanged to the empty antibonding orbitals (p^*) of the adsorbed N_2. These adsorbed N_2 (NN*) would be severely weakened and exhibited high activation due to the electron injection. It is conducive to hydrogenation for the N≡N bond to NH_3. During NRR, the crystalline phase transformation from TT-phase to T-phase leads to the decrease of V_o concentration in Nb_2O_5, thus the decreased NRR performance.

Fig. 3d shows the electron paramagnetic resonance (EPR) spectroscopy of Nb_2O_5-NCF with different NRR times. In comparison with the pristine Nb_2O_5-NCF, the V_o concentration in Nb_2O_5 obviously decreased with the NRR time, primarily owing to H^+ ions occupying the V_o sites thus resulting in the reduced active sites for N_2 adsorption and activation.

After 20 min of NRR, we replaced fresh 0.1 mol/L Na_2SO_4 electrolyte and conducted the recycling experiments using the used Nb_2O_5-NCF electrode and obtained obviously decreased NRR performance (Fig. 3e, each recycling experiment of 20 min). The above results further confirmed that with NRR time, the formation of T-phase Nb_2O_5 results in the decrease of V_o concentration, thus the reduced NRR performance. How to regenerate the electrode with high NRR activity is therefore critically important. We carried out the cyclic voltammetry (CV) experiments in 0.1 mol/L Na_2SO_4 electrolyte in the potential range from −1.2 V to 1.2 V (*vs.* RHE). The results (Fig. S7 in Supporting information) demonstrated that the oxidation peak lies at ∼ −0.5 V (*vs.* RHE), corresponding to the extraction of H^+ ions from the interlayer spacing of Nb_2O_5. The cathodic current density has a slight increase with the cycling number for Nb_2O_5-NCF and almost unchanged until 25th cycle, exhibiting an increased capacity for H^+ ions insertion. The chronoamperometric measurements were performed by applying potentials of 0.6 and −0.6 V (*vs.* RHE) for 100 s. The comparison between the anodic and cathodic current intensities indicates a faster kinetic extraction than the insertion process, exhibiting an approximate bleaching time of 15 s while the colored time of 20 s (Fig. 4a). The reversible EC results mean that the used Nb_2O_5-NCF for NRR may be regenerated to recover its high NRR activity. For this, we tried to apply an anodic potential to realize this. As expected, when an anodic potential of 1.0 V (*vs.* RHE) was applied to the used Nb_2O_5-NCF electrode for 5 min, the T-phase Nb_2O_5 with part of Nb^{4+} can be readily transformed to TT-phase Nb_2O_5 (curve II in Fig. 4b). This means that high NRR performance may be recovered by using the TT-phase Nb_2O_5 with more V_o sites. Utilizing such regeneration approach, the Nb_2O_5-NCF electrode displays superior recycling reproducibility with high NH_3 yield rate and current efficiency (Fig. 4c).

Furthermore, we found that low-temperature treatment approach (60 °C for 0.5 h) is also feasible for regeneration of the used Nb_2O_5-NCF electrode for high-performance NRR (curve III in Fig. 4b). The recycling reproducibility with high NH_3 yield rate and current efficiency was shown in Fig. 4d. The EPR measurements of Nb_2O_5-NCF sample after 120 min NRR and subsequently low temperature annealing results also confirm this (Fig. S8 in Supporting information).

In summary, highly ordered Nb_2O_5 nanochannel film (Nb_2O_5-NCF) with rich V_o was fabricated on niobium foil substrate by a facile anodization method. As a free-standing electrode for NRR, the Nb_2O_5-NCF demonstrated high electrocatalytic activity toward NH_3 synthesis. However, the NRR activity of Nb_2O_5-NCF decreased when the reaction time was over 20 min, due to a crystalline phase transformation of Nb_2O_5 from TT-phase to T-phase, resulting in the decrease of V_o concentration in Nb_2O_5, thus the reduced active sites for N_2 adsorption and activation. However, the used Nb_2O_5-NCF with decreased NRR activity could

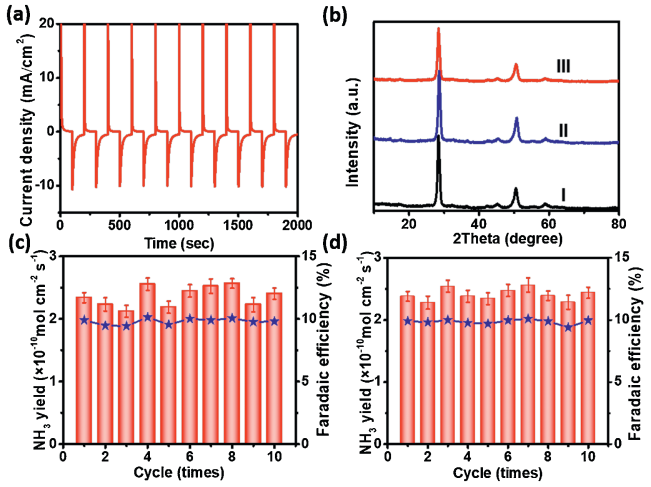

Fig. 4. (a) Chronoamperometric (CA) curves of Nb_2O_5-NCF for electrochromism (EC). (b) XRD patterns of Nb_2O_5-NCF before (curve I) and after NRR with anodizing activation (curve II) and low temperature annealing activation (curve III). Recycling test of NRR for Nb_2O_5-NCF electrode by (c) anodizing activation and (d) low temperature annealing activation.

be regenerated by applying an anodic potential or low-temperature thermal treatment approach, indicating superior recycling reproducibility with high NH_3 yield rate and current efficiency. This work provides an efficient solution to the inactivation issue of an electrocatalyst for high-performance NRR to NH_3.

Declaration of competing interest

The authors report no declarations of interest.

Acknowledgments

This work is financially supported by the National Key Research and Development Program of China (No. 2017YFA0207203) and the Natural Science Foundation of China (No. 51872292).

Appendix A. Supplementary data

Supplementary material related to this article can be found, in the online version, at doi:https://doi.org/10.1016/j.cclet.2021.01.020.

References

[1] V. Smil, Nature 400 (1999) 415–415.
[2] V. Rosca, M. Duca, M.T. de Groot, M.T.M. Koper, Chem. Rev. 109 (2009) 2209–2244.
[3] C.J. Pickett, J. Talarmin, Nature 317 (1985) 652–653.
[4] R. Zhang, Y. Zhang, X. Ren, et al., ACS Sustain. Chem. Eng. 6 (2018) 9545–9549.
[5] H. Jia, E.A. Quadrelli, Chem. Soc. Rev. 43 (2014) 547–564.
[6] M. Kitano, Y. Inoue, Y. Yamazaki, et al., Nat. Chem. 4 (2012) 934–940.
[7] K.A. Brown, D.F. Harris, M.B. Wilker, et al., Science 352 (2016) 448–450.
[8] T. Oshikiri, K. Ueno, H. Misawa, Angew. Chem. Int. Ed. 55 (2016) 3942–3946.
[9] G.N. Schrauzer, T.D. Guth, J. Am. Chem. Soc. 99 (1977) 7189–7193.
[10] Z.W. Seh, J. Kibsgaard, C.F. Dickens, et al., Science 355 (2017) 1–14.
[11] L. Wang, M. Xia, H. Wang, et al., Joule 2 (2018) 1055–1074.
[12] T.L. Frolicher, E.M. Fischer, N. Gruber, Nature 560 (2018) 360–364.
[13] Y. Yao, S. Zhu, H. Wang, H. Li, M. Shao, J. Am. Chem. Soc. 140 (2018) 1496–1501.
[14] H.K. Lee, C.S.L. Koh, Y.H. Lee, et al., Sci. Adv. 4 (2018) eaar3208.
[15] J. Kong, A. Lim, C. Yoon, et al., ACS Sustain. Chem. Eng. 5 (2017) 10986–10995.
[16] L. Zhang, X. Ji, X. Ren, et al., Adv. Mater. 30 (2018) 1800191.
[17] S. Chen, S. Perathoner, C. Ampelli, et al., Angew. Chem. Int. Ed. 56 (2017) 2699–2703.
[18] S. Mukherjee, D.A. Cullen, S. Karakalos, et al., Nano Energy 48 (2018) 217–226.
[19] W. Li, T. Wu, S. Zhang, et al., Chem. Commun. 54 (2018) 11188–11191.
[20] L. Huang, J. Wu, P. Han, et al., Small Methods 3 (2019) 1800386.
[21] R. Manjunatha, A. Karajić, V. Goldstein, A. Schechter, ACS Appl. Mater. Interfaces 11 (2019) 7981–7989.
[22] J. Han, X. Ji, X. Ren, et al., J. Mater. Chem. A 6 (2018) 12974–12977.
[23] C. Fang, T. Bi, X. Xu, et al., Adv. Mater. Interfaces 6 (2019) 1901034.
[24] W. Fu, P. Zhuang, M.O. Chee, et al., ACS Sustain. Chem. Eng. 7 (2019) 9622–9628.
[25] I. Nowak, M. Ziolek, Chem. Rev. 99 (1999) 3603–3624.
[26] W. Kong, Z. Liu, J. Han, et al., Inorg. Chem. Front. 6 (2019) 423–427.
[27] J. Han, Z. Liu, Y. Ma, et al., Nano Energy 52 (2018) 264–270.
[28] Y. Huang, Y. Zhang, X. Hu, Sol. Energy Mater. Sol. C 77 (2003) 155–162.
[29] H. Cui, G. Zhu, Y. Xie, et al., J. Mater. Chem. A 3 (2015) 11830–11837.
[30] H. Yu, L. Xu, H. Wang, et al., Electrochim. Acta 295 (2019) 829–834.
[31] M.K. Bahl, J. Phys. Chem. Solids 36 (1975) 485–491.
[32] T. Joshi, T.R. Senty, P. Borisov, A.D. Bristow, D. Lederman, J. Phys. D Appl. Phys. 48 (2015) 335308.
[33] P.L. Searle, Analyst 109 (1984) 549–568.
[34] D. Bao, Q. Zhang, F. Meng, et al., Adv. Mater. 29 (2017) 1604799.
[35] C. Shi, K. Xiang, Y. Zhu, et al., Electrochim. Acta 246 (2017) 1088–1096.
[36] R. Romero, E.A. Dalchiele, F. Martín, D. Leinen, J.R. Ramos-Barrado, Sol. Energy Mater. Sol. C 93 (2009) 222–229.